A generalized recursive convolution method for time-domain propagation in porous media

Didier Dragna, Pierre Pineau, and Philippe Blanc-BenonVEO

Citation: The Journal of the Acoustical Society of America **138**, 1030 (2015); doi: 10.1121/1.4927553
View online: http://dx.doi.org/10.1121/1.4927553
View Table of Contents: http://asa.scitation.org/toc/jas/138/2
Published by the Acoustical Society of America

A generalized recursive convolution method for time-domain propagation in porous media

Didier Dragna,[a] Pierre Pineau, and Philippe Blanc-Benon
Laboratoire de Mécanique des Fluides et d'Acoustique, Unité Mixte de Recherche, Centre National de la Recherche Scientifique 5509, École Centrale de Lyon, Université de Lyon, 36, avenue Guy de Collongue, 69134 Écully Cedex, France

(Received 2 December 2014; revised 3 April 2015; accepted 16 July 2015; published online 20 August 2015)

An efficient numerical method, referred to as the auxiliary differential equation (ADE) method, is proposed to compute convolutions between relaxation functions and acoustic variables arising in sound propagation equations in porous media. For this purpose, the relaxation functions are approximated in the frequency domain by rational functions. The time variation of the convolution is thus governed by first-order differential equations which can be straightforwardly solved. The accuracy of the method is first investigated and compared to that of recursive convolution methods. It is shown that, while recursive convolution methods are first or second-order accurate in time, the ADE method does not introduce any additional error. The ADE method is then applied for outdoor sound propagation using the equations proposed by Wilson *et al.* in the ground [(2007). Appl. Acoust. **68**, 173–200]. A first one-dimensional case is performed showing that only five poles are necessary to accurately approximate the relaxation functions for typical applications. Finally, the ADE method is used to compute sound propagation in a three-dimensional geometry over an absorbing ground. Results obtained with Wilson's equations are compared to those obtained with Zwikker and Kosten's equations and with an impedance surface for different flow resistivities.
 [http://dx.doi.org/10.1121/1.4927553]

[VEO] Pages: 1030–1042

I. INTRODUCTION

Propagation of transient signals in porous media has important practical applications, for instance, in bioacoustics to characterize bone properties (Cardoso *et al.*, 2003; Fellah *et al.*, 2004; Haïat *et al.*, 2008), in building acoustics to determine acoustic absorption of materials (Fellah *et al.*, 2003) or in outdoor sound propagation to account for the reflection of waves from the ground. For this type of signal, time-domain methods are advantageous over frequency-domain methods. The characterization of porous media in the time domain is however not straightforward, as most of the theoretical studies were conducted in the frequency domain. For instance, the Biot's equations for a viscous fluid involve frequency-dependent parameters such as the dynamic tortuosity, which lead in the time domain to convolutions or to fractional derivatives [see, e.g., Fellah *et al.* (2013)]. In outdoor sound propagation, the solid frame can be usually considered as not deformable (Attenborough *et al.*, 2011), and the behavior of porous media can be modelled with the equivalent fluid approach using various models. The Zwikker and Kosten's equations are usually chosen in the literature (Salomons *et al.*, 2002; Van Renterghem and Botteldooren, 2003), as they are simple and easy to solve numerically. However, it was shown that these equations have limited applications as they are not well-suited for a large range of grounds such as gravel, forests, or snow (Wilson *et al.*, 2007). Recently, more general time-domain equations were proposed (Wilson *et al.*, 2007; Umnova and Turo, 2009). Unlike the Zwikker and Kosten's equations, they involve convolutions, which require storing the values of the acoustic variables in the porous medium at all previous time steps in a naive approach. For a three-dimensional (3D) geometry, a tremendous memory space is thus needed. As a consequence, the use of these equations has been limited up to now to one- or two-dimensional geometries. Therefore, an efficient numerical method is necessary to evaluate convolutions with a reduced computational cost.

This problem has been thoroughly studied in electromagnetic propagation as many real materials have frequency-dependent properties. Three main methods emerged; all are based on the approximation of frequency-dependent parameters by a rational function in the frequency domain. The time-domain counterpart corresponds to a sum of exponentially decaying functions which permits a simplified computation of the convolutions. In the first method, a time discretization of the convolution is introduced. Assuming that the variables are constant over one time step or vary linearly between two consecutive time steps, the evaluation of the convolution can be reduced to that of recursive expressions. Thus, the value of the convolution at the actual time step depends on the one at the previous time step only. These methods are called recursive convolution methods (Luebbers and Hunsberger, 1992). The second method uses the Z-transform formalism to discretize in time the equations (Sullivan, 1992, 1996). As shown by Sullivan (1996), the expressions obtained are very close to those of the recursive convolution methods. In the third method, originated from the work of Joseph *et al.* (1991), a differentiation of the convolution is performed, yielding an additional set of first-order differential equations, which are

[a]Electronic mail: didier.dragna@ec-lyon.fr

 0001-4966/2015/138(2)/1030/13/$30.00

solved using the same numerical techniques as employed for the propagation equations. This method is referred to as the auxiliary differential equations (ADE) method and can be seen as a generalized recursive method as no additional approximations on the time variations of the variables are introduced.

There has already been some use of these convolution methods in acoustics. To our knowledge, the first application dates back to the work of Botteldooren (1997) which proposes a recursive convolution method to account for the effects of entropy and vorticity boundary layers on sound propagation. Later, recursive convolution methods were mainly employed to derive time-domain impedance boundary conditions, for applications in duct acoustics (Reymen *et al.*, 2008; Li *et al.*, 2012) and in outdoor sound propagation (Ostashev *et al.*, 2007; Cotté *et al.*, 2009). An ADE method was also proposed by Bin *et al.* (2009) for surface impedance implementation. The Z-transform method has received much less attention. It was used especially in duct acoustics by Özyörük and Long (1996) to derive a time-domain impedance boundary condition in a presence of a mean flow.

In addition, ADE methods are widely spread in geophysics to include effects of anelastic materials from the work of Day and Minster (1984). The impact of this paper is important, as it was referred to as a main result in a reference book on the subject (Carcione, 2001). Still for geophysics applications, the ADE method was used to compute propagation into a viscoacoustic medium (Groby and Tsogka, 2006) in which the pressure and the divergence of the displacement are related by a frequency-dependent constant. More recently, a diffusive representation for order 1/2 fractional derivatives based on the same methodology was proposed to study sound propagation in a porous medium using the Biot theory for a particular model of dynamic permeability (Blanc *et al.*, 2013).

The main objectives of this paper are to compare the accuracy of the ADE method to that of recursive convolution methods and to apply the ADE method to sound propagation in porous media. The feasibility of the approach is demonstrated on a typical outdoor sound propagation problem in a 3D configuration.

The paper is organized as follows. In Sec. II, the ADE method is described and the relation to the recursive convolution methods is highlighted. The accuracy of these various methods is then investigated. A first one-dimensional test-case is performed to numerically retrieve the order of accuracy derived analytically. In a second test-case, the error introduced by the rational function approximation is analyzed. Application of the ADE method to outdoor sound propagation is performed in Sec. III. The time-domain equations for Wilson's relaxation model are solved in the ground medium. A one-dimensional propagation calculation is first treated and the characteristics of the porous medium are retrieved. Then, the feasibility of the method for 3D geometries is demonstrated by considering the propagation of a broadband impulse signal in an inhomogeneous atmosphere.

II. RECURSIVE CONVOLUTION METHODS

A. ADE method

Time-domain equations in porous media usually involve convolutions:

$$I(u(t),t) = [u * s](t) = \int_{-\infty}^{t} u(t')s(t-t')\mathrm{d}t', \tag{1}$$

where $s(t)$ is a real and causal function and is known *a priori* and $u(t)$ is an acoustic variable, generally the pressure or the particle velocity. The function $s(t)$ is typically a relaxation function, describing the response of a porous medium to an excitation and depends on the characteristics of the porous medium. To efficiently compute the convolution, the Fourier transform of the function $s(t)$, defined by

$$\hat{s}(\omega) = \int_{-\infty}^{+\infty} s(t)e^{i\omega t}\mathrm{d}t, \tag{2}$$

is approximated by a rational function in $-i\omega$ with simple poles whose denominator and numerator are polynomials of degree P:

$$\hat{s}(\omega) \approx \hat{s}_P(\omega) = \hat{s}_\infty + \frac{a_0 + \cdots + a_{P-1}(-i\omega)^{P-1}}{1 + \cdots + b_P(-i\omega)^P}, \tag{3}$$

where $\hat{s}_\infty$ is the limit value of $\hat{s}(\omega)$ as ω tends to infinity. As $s(t)$ is a real function, all the coefficients a_i and b_i are real, and hence, the poles of $\hat{s}_P(\omega)$ are either real, denoted hereafter by λ_k, or come in complex conjugate pairs, designated by $\alpha_k \pm i\beta_k$. For causality reasons, they are located in the lower half ω-plane, which imposes that $\lambda_k \geq 0$ and $\alpha_k \geq 0$. Therefore, $\hat{s}_P(\omega)$ can be rewritten as

$$\hat{s}_P(\omega) = \hat{s}_\infty + \sum_{k=1}^{N} \frac{A_k}{\lambda_k - i\omega} + \sum_{k=1}^{M} \frac{1}{2}\left[\frac{B_k + iC_k}{\alpha_k + i\beta_k - i\omega} + \frac{B_k - iC_k}{\alpha_k - i\beta_k - i\omega}\right], \tag{4}$$

with $P = N + 2M$ and where A_k, B_k, and C_k are numerical parameters. In the time domain, the approximation is written as

$$s(t) \approx \hat{s}_\infty \delta(t) + \sum_{k=1}^{N} A_k e^{-\lambda_k t}\mathrm{H}(t) + \sum_{k=1}^{M} e^{-\alpha_k t}[B_k \cos(\beta_k t) + C_k \sin(\beta_k t)]\mathrm{H}(t), \tag{5}$$

where $\delta(t)$ and $H(t)$ stand for the Dirac and Heaviside functions, respectively. A physical interpretation of each term can be provided. As $\hat{s}_\infty$ is the high-frequency limit of $\hat{s}(\omega)$, the first term corresponds to the instantaneous response to the excitation. The second term is a classical relaxation function which decays exponentially with time and whose time constant is equal to $1/\lambda_k$. Finally, the third term is an

oscillatory response damped with time. The period of oscillations is governed by the imaginary part of the pole β_k and the decay with time by its real part α_k. The approximation of $\hat{s}(\omega)$ by a rational function can be obtained using various numerical methods. Among them, the vector fitting method proposed by Gustavsen and Semlyen (1999) is used hereafter.

Introducing the approximation of $s(t)$ given in Eq. (5) into Eq. (1) leads to

$$I(u(t),t) = \hat{s}_\infty u(t) + \sum_{k=1}^{N} A_k \phi_k(t) + \sum_{k=1}^{M} [B_k \psi_k^{(1)}(t) + C_k \psi_k^{(2)}(t)], \tag{6}$$

where the auxiliary functions $\phi_k(t)$, $\psi_k^{(1)}(t)$, and $\psi_k^{(2)}(t)$, also referred to as accumulators or memory variables in geophysics, are given by the convolutions

$$\phi_k(t) = \int_{-\infty}^{t} u(t') e^{-\lambda_k (t-t')} \mathrm{d}t', \tag{7}$$

$$\psi_k^{(1)}(t) = \int_{-\infty}^{t} u(t') e^{-\alpha_k (t-t')} \cos(\beta_k (t-t')) \mathrm{d}t', \tag{8}$$

$$\psi_k^{(2)}(t) = \int_{-\infty}^{t} u(t') e^{-\alpha_k (t-t')} \sin(\beta_k (t-t')) \mathrm{d}t'. \tag{9}$$

By differentiating Eqs. (7)–(9), it is straightforwardly deduced that these auxiliary functions satisfy the following equations:

$$\frac{\partial \phi_k}{\partial t} + \lambda_k \phi_k(t) = u(t), \tag{10}$$

$$\frac{\partial \psi_k^{(1)}}{\partial t} + \alpha_k \psi_k^{(1)}(t) + \beta_k \psi_k^{(2)}(t) = u(t), \tag{11}$$

$$\frac{\partial \psi_k^{(2)}}{\partial t} + \alpha_k \psi_k^{(2)}(t) - \beta_k \psi_k^{(1)}(t) = 0. \tag{12}$$

This method is referred to as the ADE method because additional first-order differential equations are solved using standard numerical techniques, instead of computing directly the convolutions and of storing the time evolution of the variable u in the numerical domain.

B. Recursive convolution methods and relation to the ADE method

Recursive convolution methods are an alternative to the ADE method. Instead of integrating first-order equations, the time evolution of the auxiliary functions is obtained from recursive expressions relating values at two consecutive time steps. These expressions are obtained from those of the ADE methods. Thus, the equation for ϕ_k in Eq. (10) is first written in the form

$$\frac{\partial}{\partial t}\left[e^{\lambda_k t} \phi_k\right] = e^{\lambda_k t} u(t). \tag{13}$$

Then, discretizing in time the problem with an uniform time step Δt and integrating over two consecutive time steps $n\Delta t$ and $(n+1)\Delta t$, with n an integer, lead to the relation

$$\phi_k[(n+1)\Delta t] = e^{-\lambda_k \Delta t} \phi_k[n\Delta t] + e^{-\lambda_k \Delta t} \int_0^{\Delta t} e^{\lambda_k t'} u[t + n\Delta t] \mathrm{d}t'. \tag{14}$$

This formula is the basis of most recursive convolution methods. Indeed, assuming that $u(t)$ is constant in the interval $[n\Delta t, (n+1)\Delta t]$ and is equal to $u[(n+1)\Delta t]$ gives the piecewise constant recursive convolution (PCRC) method (Luebbers and Hunsberger, 1992):

$$\phi_k^{\mathrm{PCRC}}[(n+1)\Delta t] = e^{-\lambda_k \Delta t} \phi_k^{\mathrm{PCRC}}[n\Delta t] + \frac{1 - e^{-\lambda_k \Delta t}}{\lambda_k} u[(n+1)\Delta t]. \tag{15}$$

Similarly, the trapezoidal recursive convolution (TRC) method (Siushansian and LoVetri, 1997) is obtained by assuming that $u(t)$ is constant in the interval $[n\Delta t, (n+1)\Delta t]$ and is equal to $(u[n\Delta t] + u[(n+1)\Delta t])/2$. Finally, in the piecewise linear recursive convolution (PLRC) method (Kelley and Luebbers, 1996), u is approximated by a linear function in the interval $[n\Delta t, (n+1)\Delta t]$.

Introducing $\psi_k = \psi_k^{(1)} + i\psi_k^{(2)}$, a similar expression is obtained from Eqs. (11) and (12) in the case of a complex conjugate pair of poles:

$$\psi_k[(n+1)\Delta t] = e^{-(\alpha_k + i\beta_k)\Delta t} \psi_k[n\Delta t] + e^{-(\alpha_k + i\beta_k)\Delta t} \int_0^{\Delta t} e^{(\alpha_k + i\beta_k)t'} u[t + n\Delta t] \mathrm{d}t'. \tag{16}$$

C. Error introduced by recursive convolution methods

Unlike the ADE method, recursive convolution algorithms introduce additional approximations on the variation of $u(t)$ during one time step. It is then interesting to determine the errors generated by these approximations. Thus, one considers $u(t)$ to be a time harmonic function, i.e., $u(t) = e^{-i\omega t}$. For the sake of simplicity, only real poles are considered hereafter but the results can be extended straightforwardly to complex conjugate poles. In this case, from Eq. (10), the auxiliary function ϕ_k is given by

$$\phi_k(t) = \frac{1}{\lambda_k - i\omega} e^{-i\omega t}. \tag{17}$$

The analytical values of ϕ_k for the recursive convolution methods can be obtained from the recursive formula in Eq. (14). For example, the PCRC method leads for a harmonic function $u(t)$ to

$$\phi_k^{\mathrm{PCRC}}(t) = \frac{1 - e^{-\lambda_k \Delta t}}{\lambda_k} e^{-i\omega t} + e^{-\lambda_k \Delta t} \phi_k^{\mathrm{PCRC}}(t - \Delta t). \tag{18}$$

The auxiliary function ϕ_k^{PCRC} can then be expressed as a geometric series:

$$\phi_k^{\mathrm{PCRC}}(t) = \frac{1 - e^{-\lambda_k \Delta t}}{\lambda_k} e^{-i\omega t} \sum_{n=0}^{+\infty} e^{(-\lambda_k \Delta t + i\omega \Delta t)n}, \tag{19}$$

which leads to the expression

$$\phi_k^{\mathrm{PCRC}}(t) = \frac{1 - e^{-\lambda_k \Delta t}}{\lambda_k} e^{-i\omega t} \frac{1}{1 - e^{-\lambda_k \Delta t + i\omega \Delta t}}. \tag{20}$$

The auxiliary function in the PCRC approximation can then be expressed as a function of the exact value of the auxiliary function by

$$\phi_k^{\mathrm{PCRC}}(t) = \phi_k(t) \frac{1 - e^{-\lambda_k \Delta t}}{\lambda_k \Delta t} \frac{\lambda_k \Delta t - i\omega \Delta t}{1 - e^{-\lambda_k \Delta t + i\omega \Delta t}}. \tag{21}$$

To determine the order of the approximation of the PCRC method, a Taylor expansion in Δt of the preceding equation is performed yielding

$$\phi_k^{\mathrm{PCRC}}(t) = \phi_k(t) \left[1 - \frac{i\omega \Delta t}{2} + O(\Delta t^2) \right]. \tag{22}$$

This shows that the PCRC is only a first-order approximation. Therefore, when employing high-order time-integration schemes, the use of the PCRC method is expected to deteriorate the accuracy. Similarly, for the TRC and PLRC methods, one gets the following estimates:

$$\phi_k^{\mathrm{TRC}}(t) = \phi_k(t) \left[1 + \frac{\lambda_k \Delta t}{12} i\omega \Delta t - \frac{(\omega \Delta t)^2}{12} + O(\Delta t^3) \right], \tag{23}$$

$$\phi_k^{\mathrm{PLRC}}(t) = \phi_k(t) \left[1 - \frac{(\omega \Delta t)^2}{12} + O(\Delta t^3) \right]. \tag{24}$$

This shows that the TRC method is a second-order method, as the error decreases as Δt^2. The PLRC method is also a second-order method and has a slightly better accuracy than the TRC method.

D. Test-case

1. Accuracy of the recursive convolution algorithms

In this section, a test-case is performed to validate the methods presented previously and to investigate their accuracy. For this purpose, one considers the equation

$$\frac{\partial p}{\partial t} + c \frac{\partial p}{\partial x} + \hat{b}_\infty p - \hat{b}_\infty \lambda \phi = 0, \tag{25}$$

with $\hat{b}_\infty = 0.01$, $c = 1$, and $\lambda = 1$ and

$$\phi(t) = \int_0^t e^{-\lambda(t-t')} p(t') \mathrm{d}t'. \tag{26}$$

This corresponds to the advection equation

$$\frac{\partial p}{\partial t} + c \frac{\partial p}{\partial x} + b * p = 0, \tag{27}$$

with an additional frequency-dependent dissipative term $b(t)$ whose Fourier transform is given by

$$\hat{b}(\omega) = \hat{b}_\infty \frac{-i\omega}{\lambda - i\omega}. \tag{28}$$

At low frequencies, the dissipative term is almost zero while at high frequencies, it tends to the constant value $\hat{b}_\infty$. The frequency variation of $\hat{b}(\omega)$ between these two limits is governed by the parameter λ. The initial disturbances are given by

$$p(x, t = 0) = \left(1 - 2 \frac{x^2}{B^2} \right) \exp\left(- \frac{x^2}{B^2} \right), \tag{29}$$

with $B = 2.5$ and the solution is advanced to $t = 100$. The spatial differentiation is calculated using a Fourier pseudo-spectral method [see, e.g., Boyd (2001)] to ensure a negligible error. The mesh size is $\Delta x = 1$. The time integration is performed using a low storage fourth-order Runge-Kutta algorithm (Berland *et al.*, 2006). Using recursive convolution methods, the term $-\hat{b}_\infty \lambda \phi$ in Eq. (25) is integrated in first order according to time after updating the auxiliary function ϕ.

The time series of the solution at the initial and final times are represented as a function of x in Fig. 1. The analytical solutions for ϕ and p are given in Appendix A. The initial disturbances are symmetrical around $x = 0$ and the maximum amplitude is equal to unity. At $t = 100$, the maximal amplitude is strongly reduced as it is equal to 0.6 due to the dissipative term. Moreover, the shape of the time series is modified as the solution is no longer symmetrical. This is related to the frequency variations of $\hat{b}(\omega)$. The numerical solutions obtained at $t = 100$ for a time step $\Delta t = 0.5$ using the PCRC and ADE methods are also represented in Fig. 1(b). It is seen that the numerical solution using the ADE method is almost superimposed on the analytical solution, while discrepancies are observed when using the PCRC method. The curves obtained for the TRC and PLRC methods are not represented as they are similar to that obtained for the ADE method.

A time-step convergence study is carried out to illustrate the accuracy of the various methods. The error ϵ on a quantity of interest u is calculated with the formula

$$\epsilon[u] = \sqrt{\int_D |u_{\mathrm{ana}}(x, t = 100) - u(x, t = 100)|^2 \mathrm{d}x}, \tag{30}$$

where u_{ana} is the analytical solution. The error on ϕ is displayed in Fig. 2(a) as a function of the normalized time step $\mathrm{CFL} = c\Delta t/\Delta x$, which corresponds to the Courant-Friedrichs-Lewy number, for the different methods. The order of the recursive convolution methods, obtained analytically in Sec. II C is retrieved. Thus, the PCRC method is a first-order method while the TRC and PLRC methods are second-order accurate in time. Note also the error is smaller using the

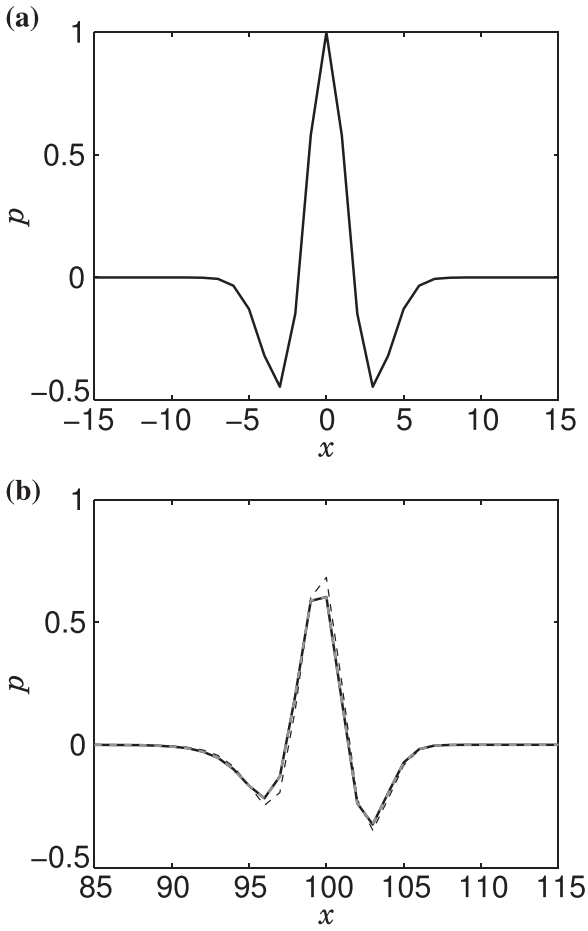

FIG. 1. Time series of p (a) at the initial time and (b) at the final time $t = 100$ as a function of x: (black solid line) analytical solution and numerical solutions using (black dashed line) the PCRC method and (gray dashed line) the ADE method.

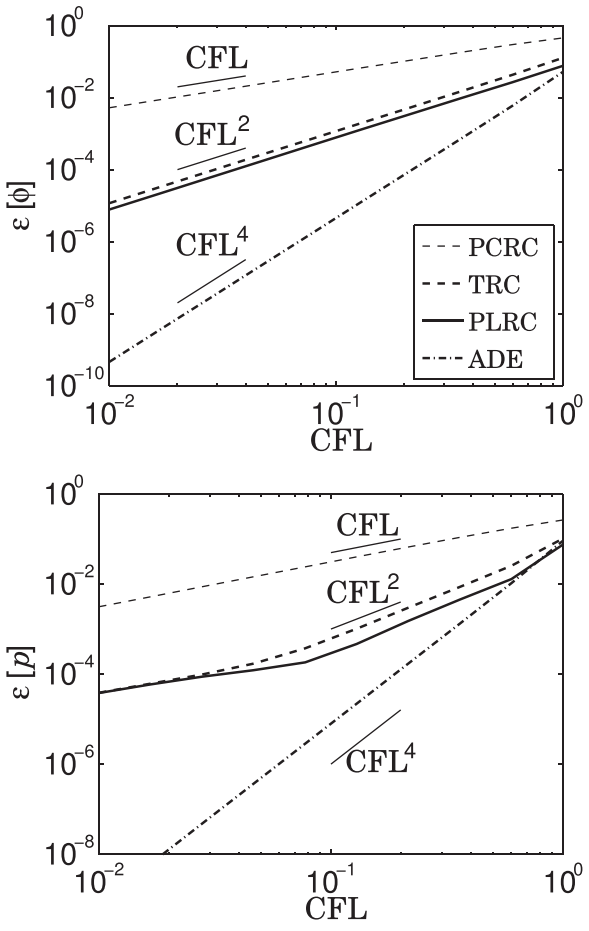

FIG. 2. Error on (a) ϕ and (b) p as a function of the normalized time step $\mathrm{CFL} = c\Delta t/\Delta x$ using (thin dashed line) the PCRC method, (thick dashed line) the TRC method, (solid line) the PLRC method, and (dashed-dotted line) the ADE method.

PLRC method than the TRC method. In addition, the order of accuracy of the ADE method corresponds to that of the time-integration algorithm. In this case, as a fourth-order Runge-Kutta scheme is used, it is seen that the ADE method is fourth-order accurate. Concerning the error on p plotted as a function of the normalized time step in Fig. 2(b), the accuracy of the solution is strongly dependent on the accuracy of ϕ and, in most of the cases, the order of accuracy of p is that of ϕ. Thus, using the PCRC and ADE methods, p is first- and fourth-order accurate in time, respectively. For the TRC and PLRC methods, the solution is second-order accurate in time except for the PLRC method with CFL smaller than 0.03, for which first-order accuracy is observed. This behavior is related to the first-order time-integration scheme used for the term $-b\lambda\phi$.

2. Accuracy of the approximation by a rational function

In this section, the influence of the approximation of a relaxation function by a rational function on the accuracy is investigated. With this aim, one considers the advection of acoustic waves in a porous medium with an air flow resistivity σ_0, a tortuosity q, and porosity Ω, using one of the simplest models, which is the Zwikker and Kosten's model. In the frequency-domain, the sound pressure is written as

$$\frac{\partial \hat{p}}{\partial x} - ik(\omega)\hat{p} = 0, \tag{31}$$

where the acoustic wavenumber $k(\omega)$ is given by (Salomons, 2001)

$$k(\omega) = \frac{\omega q}{c}\sqrt{1 + \frac{\omega_0}{-i\omega}}, \tag{32}$$

with $\omega_0 = \sigma_0\Omega/(\rho_0 q^2)$. Multiplying both sides of Eq. (31) by $\sqrt{1 + \omega_0/(-i\omega)}$ leads to

$$-i\omega\hat{p} + \frac{c}{q}\sqrt{1 + \frac{\omega_0}{-i\omega}}\frac{\partial \hat{p}}{\partial x} + \omega_0 p = 0, \tag{33}$$

which is written back in the time domain as

$$\frac{\partial p}{\partial t} + \frac{c}{q}\left[s * \frac{\partial p}{\partial x}\right] + \omega_0 p = 0, \tag{34}$$

where the relaxation function $s(t)$ is the inverse Fourier transform of

$$\hat{s}(\omega) = \sqrt{1 + \frac{\omega_0}{-i\omega}}. \tag{35}$$

The parameter ω_0 is a characteristic of the medium which separates two regimes. For $\omega \ll \omega_0$, the advection equation can be written as a diffusion equation:

$$\frac{\partial p}{\partial t} - D\frac{\partial^2 p}{\partial x^2} = 0, \tag{36}$$

with a diffusivity coefficient $D = c^2/(q^2\omega_0)$. For $\omega \gg \omega_0$, the advection equation has the simple form

$$\frac{\partial p}{\partial t} + \frac{c}{q}\frac{\partial p}{\partial x} + \omega_0 p = 0, \tag{37}$$

whose solutions are evanescent waves which propagated at a sound speed c/q and whose damping is related to ω_0.

As in the previous test-case, a Fourier pseudospectral method is used. The characteristics of the porous medium are set to $\sigma_0 = 10\,\text{kPA s m}^{-2}$, $q = 1.8$, and $\Omega = 0.5$. The mesh size is uniform with $\Delta x = 0.0085\,\text{m}$. The initial perturbations are given by

$$p(x, t = 0) = C\cos\left(\frac{2\pi x}{A}\right)\exp\left(-\frac{x^2}{B^2}\right), \tag{38}$$

with $C = 1\,\text{Pa}$, $A = 4\Delta x$, and $B = 6\Delta x$. The solution is advanced up to $t = 0.003\,\text{s}$. The time step is set to $2.5 \times 10^{-5}\,\text{s}$ and the CFL number $\text{CFL} = c_0\Delta t/\Delta x$ is equal to one. The ADE method is used to handle the convolution. Therefore, instead of considering Eq. (34), the following first-order equations are solved:

$$\frac{\partial p}{\partial t} + \frac{c}{q}\frac{\partial p}{\partial x} + \frac{c}{q}\sum_{k=1}^{N} A_k\phi_k + \omega_0 p = 0, \tag{39}$$

$$\frac{\partial \phi_k}{\partial t} + \lambda_k\phi_k = \frac{\partial p}{\partial x}, \tag{40}$$

where a rational function with real poles only is used to approximate $\hat{s}(\omega)$:

$$\hat{s}(\omega) \approx \hat{s}_N(\omega) = 1 + \sum_{k=1}^{N}\frac{A_k}{\lambda_k - i\omega}. \tag{41}$$

The vector fitting algorithm is employed to get the coefficients A_k and λ_k and is initialized using a vector of 100 logarithmically spaced frequencies f_i between 50 Hz and 20 kHz. The number of poles N is chosen between 1 and 10. The relative error over the whole frequency band of interest, computed with

$$\epsilon[\hat{s}] = \sum_{i=1}^{100}(\hat{s}(\omega_i) - \hat{s}_N(\omega_i))^2 \Big/ \sum_{i=1}^{100}(\hat{s}(\omega_i) - 1)^2, \tag{42}$$

is represented as a function of N on a logarithmic scale along the vertical axis in Fig. 3. It is observed that the error decreases exponentially with the number of poles. Thus, the approximation error is large using only one pole, about 21.1% but is greatly reduced as N increases. Therefore, it is equal to 3.82% for $N = 2$ and to 0.7% only for $N = 3$.

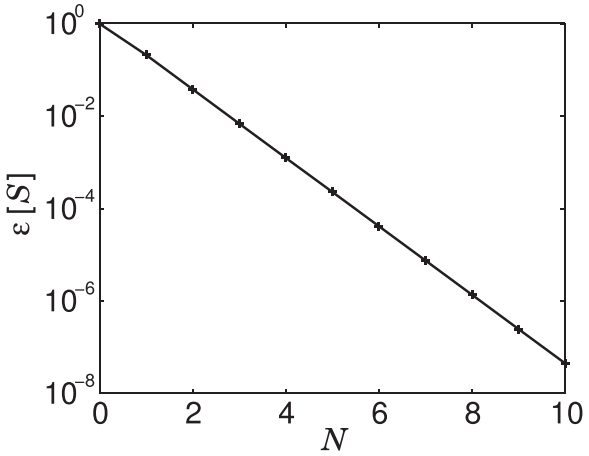

FIG. 3. Error on the relaxation function as a function of the number of poles.

The solutions obtained from both the analytical solution given in Appendix B and the numerical solutions at the final time for various number of poles in the rational function approximation are represented as a function of x in Fig. 4. The amplitude of the numerical solution obtained by neglecting the convolution, which corresponds to the case $N = 0$, is smaller than that of the analytical solution. Thus, the maximal amplitude is 0.15 Pa for the analytical solution and only 0.03 Pa for the numerical solution. This shows that the convolution term has a strong influence on the numerical solution. Using only one pole for the recursive convolution method allows one to reduce the discrepancies as the maximal amplitude for the numerical solution is now 0.12 Pa. For $N \geq 2$, the amplitude obtained analytically is retrieved and the analytical and numerical solutions are almost superimposed.

As done in Sec. II D 1, a time-step convergence analysis is performed. The error is computed at the final time $t = 0.003\,\text{s}$, using Eq. (30). It is plotted as a function of the normalized time step $\text{CFL} = c\Delta t/\Delta x$ in Fig. 5 for various numbers of poles. For small values of N, i.e., $N = 0$ and $N = 1$, the error does not depend on the time step. It is mostly generated by the omission of the convolution for $N = 0$ or by the inaccurate approximation of the relaxation function by a

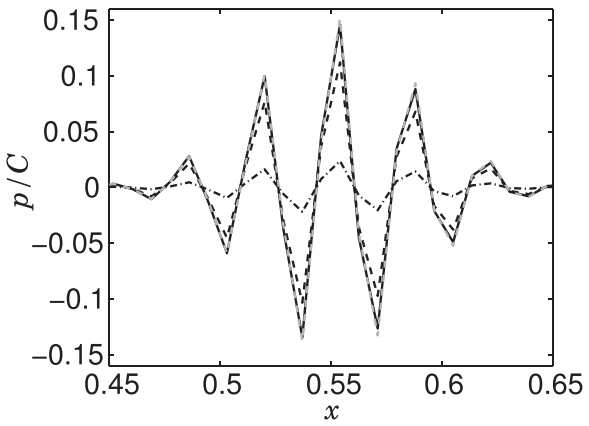

FIG. 4. Time series of p for (gray dashed line) the analytical solution and for the numerical solution (black dashed-dotted line) without the convolution term and with the convolution term with (black dashed line) one pole and (black solid line) two poles.

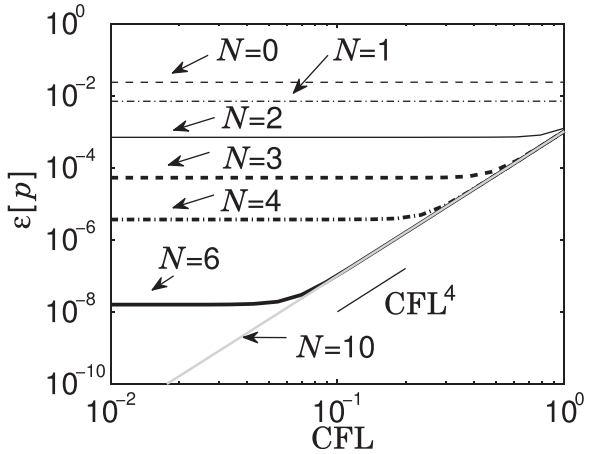

FIG. 5. Error on p as a function of the normalized time step $\mathrm{CFL} = c_0\Delta t/\Delta x$ for various numbers of poles: (black thin dashed line) $N = 0$, (black thin dashed-dotted line) $N = 1$, (black thin solid line) $N = 2$, (black thick dashed line) $N = 3$, (black thick dashed-dotted line) $N = 4$, (black thick solid line) $N = 6$, and (gray thick solid line) $N = 10$.

rational function with only one pole for $N = 1$. Therefore, reducing the time step does not allow us to reduce the error in these cases. For larger values of N, which are $N = 2$, 3, 4 and 6, the variations of the error with the CFL present similar shapes. For large CFL, the error decreases as $(\Delta t)^4$, which is expected as a fourth-order time-integration algorithm is used. As the CFL is reduced, the error reaches a plateau, and does not depend anymore of the CFL but only on the number of poles. For instance, it is equal to 7×10^{-4} for $N = 2$ and is reduced to 5×10^{-5}, 4×10^{-6}, and 1.6×10^{-8} for $N = 3$, 4, and 6, respectively. For N sufficiently large, $N > 10$ in this case, the error curve is a straight line. Indeed, the rational function approximation of the relaxation function is accurate enough so that the error is mainly generated by the time-integration method.

III. APPLICATION TO OUTDOOR SOUND PROPAGATION

In this section, the ADE method is employed for studying sound propagation in an inhomogeneous atmosphere.

A. Numerical aspects

1. Equations

In the air, a set of coupled equations for the acoustic pressure p and acoustic particle velocity $\mathbf{v}$ accounting for a mean flow $\mathbf{V}_0$ are solved (Ostashev *et al.*, 2005). They correspond to the linearized Euler equations with the omission of terms of order $(|\mathbf{V}_0|/c)^2$. In the porous medium, the time-domain equations for the Wilson's relaxation model are solved. They are given by (Wilson *et al.*, 2007)

$$\frac{\partial \mathbf{v}}{\partial t} + \frac{\Omega}{\rho_0 q^2}[s^v * \nabla p] + \frac{1}{\tau_v}\mathbf{v} = \mathbf{0}, \tag{43}$$

$$\frac{\partial p}{\partial t} + \frac{\rho_0 c^2}{\Omega}[s^e * (\nabla \cdot \mathbf{v})] = 0, \tag{44}$$

where the functions s^v and s^e,

$$s^v = \delta(t) - \frac{1}{2}\, s\left(\frac{t}{\tau_v}, 1\right), \tag{45}$$

$$s^e = \delta(t) - \frac{\gamma - 1}{\gamma}\, s\left(\frac{t}{\tau_e}, \gamma - 1\right), \tag{46}$$

describe the viscous and thermal diffusion processes in the porous medium, with characteristic relaxation times τ_v and τ_e, respectively. They are related to the characteristics of the medium with $\tau_v = 2\rho_0 q^2/(\Omega\sigma_0)$ and $\tau_e = \mathrm{P_r} s_B^2 \tau_v$ (Wilson *et al.*, 2007), where $\mathrm{P_r}$ is the Prandtl number and s_B is a pore shape factor set to one hereafter. The function $s(t/\tau, a)$ in Eqs. (45) and (46) is a general relaxation function such as its Fourier transform $\hat{s}(\omega\tau, a)$ is written as

$$\hat{s}(\omega\tau, a) = \frac{1 + a}{\sqrt{1 - i\omega\tau} + a}. \tag{47}$$

Applying the ADE method to the Wilson's equations lead to the resolution of the set of four equations:

$$\frac{\partial \mathbf{v}}{\partial t} + \frac{\Omega}{\rho_0 q^2}\nabla p + \frac{\Omega}{\rho_0 q^2}\sum_{k=1}^{N^v} A_k^v \boldsymbol{\phi}_{\boldsymbol{k}}^{\boldsymbol{v}} + \frac{1}{\tau_v}\mathbf{v} = \mathbf{0}, \tag{48}$$

$$\frac{\partial p}{\partial t} + \frac{\rho_0 c^2}{\Omega}\nabla \cdot \mathbf{v} + \frac{\rho_0 c^2}{\Omega}\sum_{k=1}^{N^e} A_k^e \phi_k^e = 0, \tag{49}$$

$$\frac{\partial \boldsymbol{\phi}_{\boldsymbol{k}}^{\boldsymbol{v}}}{\partial t} + \lambda_k^v \phi_k^v = \nabla p, \tag{50}$$

$$\frac{\partial \phi_k^e}{\partial t} + \lambda_k^e \phi_k^e = \nabla \cdot \mathbf{v}, \tag{51}$$

where the relaxation functions have been approximated using real poles only:

$$\hat{s}^v(\omega) \approx 1 + \sum_{k=1}^{N^v} \frac{A_k^v}{\lambda_k^v - i\omega}, \tag{52}$$

$$\hat{s}^e(\omega) \approx 1 + \sum_{k=1}^{N^e} \frac{A_k^e}{\lambda_k^e - i\omega}. \tag{53}$$

2. Numerical techniques

The Fourier pseudospectral method offers advantages compared to finite difference methods, as spatial derivatives are accurately evaluated using only two points per wavelength. However, it requires the solution to be periodic in space and smooth. The accuracy of the Fourier pseudospectral method is therefore seriously degraded by the presence of discontinuities. An extended Fourier pseudospectral method was recently proposed to handle fluid media with piecewise homogeneous properties (Hornikx *et al.*, 2010) but cannot be applied to our case, as the porous medium properties are frequency-dependent and can also vary in space. Therefore, the spatial derivatives in the direction perpendicular to the interface between the air and the porous medium are evaluated using optimized fourth-order finite

difference schemes (Bogey and Bailly, 2004) previously employed in outdoor sound propagation studies (Dragna *et al.*, 2011, 2013). These schemes allow us to calculate acoustic wavelength down to five or six points per wavelength. In the directions parallel to the ground interface, the Fourier pseudospectral method is used.

As the equations governing sound propagation in the air and in the porous medium are different, the numerical domain is split into two subdomains, one for the air and one for the porous medium. At the interface between the two subdomains, a patching technique based on the characteristic variables [as described, for instance, in Hornikx (2009)] is employed. It is detailed in Appendix C. At the outer boundaries, perfectly matched layers in the split version as in Hornikx *et al.* (2010) are used.

B. One-dimensional test case

A one-dimensional test-case is first performed. The parameters of the porous medium are set to $\sigma_0 = 10\,\text{kPa s m}^{-2}$, $q = 1.8$, and $\Omega = 0.5$. The two relaxation functions are approximated using 5 real poles on the frequency band between 50 Hz and 20 kHz. In addition to the acoustic pressure and velocity, there are thus for a one-dimensional test-case ten supplementary variables in the porous medium to store. Compared to a direct evaluation of convolutions or to more sophisticated methods, the recursive convolution methods allows one to save a very large memory space and also computational time. For instance, for the same case and for a frequency of 800 Hz, Wilson *et al.* (2007) need 800 additional terms for evaluating each convolution. Increasing the frequency would even require to store more and more terms. The porous and air media are located at $x<0$ and $x>0$, respectively. The mesh grid in the porous and air media is uniform and the corresponding spatial steps are $\Delta x_p = 0.0014\,\text{m}$ and $\Delta x_a = 0.0028\,\text{m}$, respectively. In the air domain, this corresponds to a minimum of six points per wavelength, which is necessary for accuracy, as indicated in the preceding paragraph. The mesh size in the porous medium is smaller, as the non-centered finite-difference schemes used at the interface are quite dissipative for small wavelengths and add a significant attenuation to that due to the porous medium. As shown later, a resolution of 12 points per wavelength is sufficient so that the numerical attenuation of the signal in the porous medium corresponds to the theoretical attenuation. There are 1000 and 1225 points in the air and in the porous medium, respectively. The CFL number is set to unity. An impulse source similar to that in Eq. (29) is used with $B = 3\Delta x_a$, and is located initially at $x_S = 1\,\text{m}$.

To validate the implementation of the Wilson's relaxation equations, the characteristic impedance of the medium is computed and compared to the analytical expression:

$$Z_W = \frac{q\rho_0 c_0}{\Omega}\left[\left(1+\frac{\gamma-1}{\sqrt{1-i\omega\tau_e}}\right)\left(1-\frac{1}{\sqrt{1-i\omega\tau_v}}\right)\right]^{-1/2}. \tag{54}$$

Thus, a Fourier transform of the acoustic pressure and velocity, denoted by $\hat{p}$ and $\hat{v}$, at a node located at $x=-0.25\,\text{m}$ is performed. The characteristic impedance Z is then obtained by computing the ratio between these two quantities, i.e., $Z=-\hat{p}/\hat{v}$. The minus sign is necessary as the wave propagates toward negative x. The real and imaginary parts of Z are represented as a function of the frequency along with those of the analytical expression in Fig. 6. A good accordance is obtained over the whole frequency band of interest.

A further validation is performed by comparing the attenuation of the signal inside the porous medium. As proposed in Wilson *et al.* (2007), the attenuation is computed at two consecutive grid nodes in the porous medium with $\alpha = \log[\hat{p}(\omega,x+\Delta x)/\hat{p}(\omega,x)]/\Delta x$. It is plotted as a function of the frequency in Fig. 7. The analytical expression of $\alpha = \text{Im}[k_W]$, with

$$k_W = \frac{q\omega}{c_0}\left[\left(1+\frac{\gamma-1}{\sqrt{1-i\omega\tau_e}}\right)\Big/\left(1-\frac{1}{\sqrt{1-i\omega\tau_v}}\right)\right]^{1/2}, \tag{55}$$

is also represented in Fig. 7. The agreement between the numerical and analytical solutions is satisfactory up to the maximal frequency of interest.

C. 3D application

In this section, the ADE method is employed to study sound propagation in an inhomogeneous atmosphere and in a 3D geometry. The vertical sound speed profile is given by

$$c(z) = c_0 + a_c \log\frac{z+z_0}{z_0}, \tag{56}$$

with $c_0 = 340\,\text{m s}^{-1}$, $a_c = 2\,\text{m s}^{-1}$, and $z_0 = 0.1\,\text{m}$. The air density is set to $\rho_0 = 1.22\,\text{kg m}^3$. For the ground, a rigidly backed layer of thickness 0.1 m is used. The ground porosity and tortuosity are set to 0.5 and 1.8, respectively. The flow resistivity is first set to $10\,\text{kPa s m}^{-2}$ and second to 200 kPa s m^{-2}. Three different modelings of the ground effects are considered. In the first one, the Wilson's equations are solved in the ground, while in the second one, the Zwikker

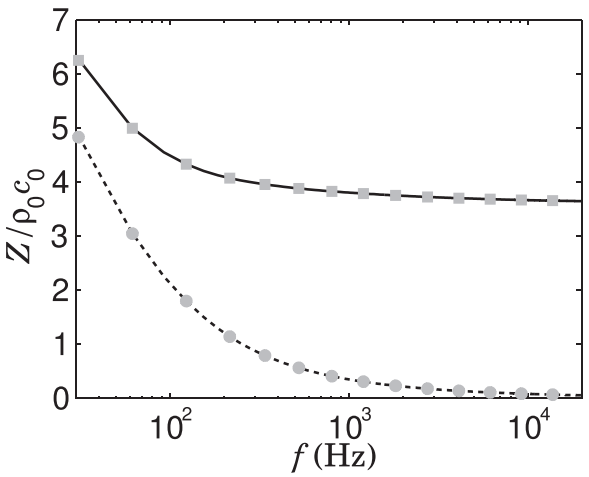

FIG. 6. Real and imaginary parts of the normalized impedance of the porous medium obtained (solid and dashed lines, respectively) analytically and (square and circles, respectively) from the numerical solution.

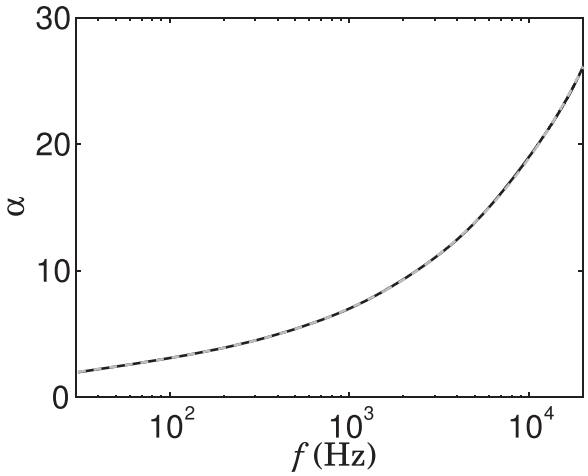

FIG. 7. Attenuation spectra for (solid line) the numerical solution and (dashed line) the analytical solution.

and Kosten's equations are employed. In the third one, the propagation of acoustic waves in the ground is not modelled and surface impedance corresponding to the Wilson relaxation model of a rigidly backed layer is used. This is done employing a time-domain impedance boundary condition presented in Cotté *et al.* (2009) and Dragna *et al.* (2013). For configurations where propagation equations in the ground are solved, the grid has $1536 \times 128 \times 734$ points which corresponds to a total of more than 144×10^6 of points. The spatial step is $\Delta x = \Delta y = 0.1$ m in the x- and y-directions along which the Fourier pseudospectral method is used. In the z-direction, finite difference schemes are employed with a reduced accuracy and the spatial step is diminished to $\Delta z_a = 0.035$ m in the air and to $\Delta z_p = 0.008$ m in the porous medium. A schematic of the grid in the x-z plane is represented in Fig. 8. For configurations using the impedance boundary condition, the grid is similar except that the porous medium is not modelled. The time step is chosen as 2.45×10^{-5} s. The simulation is initialized by setting

$$\mathbf{v}(t=0) = \mathbf{0}, \tag{57}$$

$$p(t=0) = \rho_0 c_0^2 \exp\left(-\frac{x^2 + y^2 + (z - z_S)^2}{B^2}\right), \tag{58}$$

with $B = 0.24$ m and where the height of the source is $z_S = 1$ m. The simulations are run up to $t = 0.47$ s. It is worthwhile noting that the increase in memory space due to the addition of the auxiliary functions for computing the convolutions is only 4% in this case.

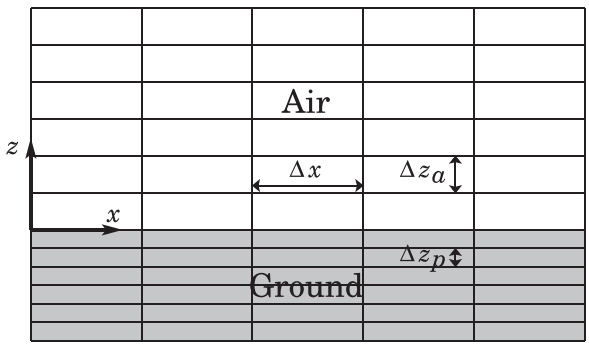

FIG. 8. Schematic in the (x, z) plane of the mesh grid used for the 3D computation.

First, the results obtained for the air flow resistivity $\sigma_0 = 10$ kPa s m^{-2} are considered. The time series of the pressure at a receiver located at $x = 150$ m, $y = 0$ m, and $z = 2$ m are represented in Fig. 9(a) for the three models. The first arrival around $t = 0.432$ s corresponds to the direct wave and is thus the same in the three cases. Later arrivals around $t = 0.434$ s related to reflected waves from the ground are similar when solving the Wilson's equations in the ground and using an impedance condition with the Wilson model. Discrepancies are however observed when solving the Zwikker and Kosten's equations in the ground. The last arrival after $t = 0.44$ s is a low-frequency oscillating wave, typical of a surface wave. This component is different in the three cases. The energy spectral density (ESD) of the signals is plotted as a function of the frequency in Fig. 9(b). For low frequencies ($f \lesssim 700$ Hz), the ESD obtained by solving the Wilson's equations in the ground and obtained by using an impedance condition with the Wilson's model are in good agreement. For higher frequencies, large discrepancies are observed. Indeed, for this low flow resistivity, the local

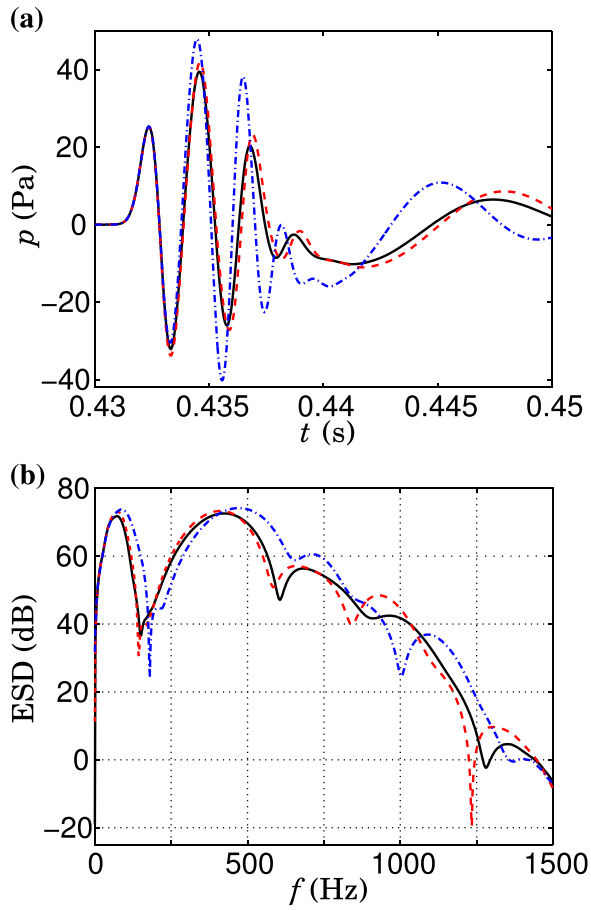

FIG. 9. (Color online) (a) Time series of the pressure and (b) corresponding energy spectral densities obtained at a receiver located at $x = 150$ m, $y = 0$ m, and $z = 2$ m for the three ground modelling: propagation in the ground using the (solid line) Wilson's and (dashed-dotted line) Zwikker and Kosten's equations or (dashed line) impedance boundary condition using the Wilson's model. The air flow resistivity of the ground is set to $\sigma_0 = 10$ kPa s m^{-2}. The reference for the dB calculation is 4×10^{-10} Pa^2 s^2.

reaction assumption is expected to be not valid. Concerning the ESD obtained with the Zwikker and Kosten's equations, it is seen that the results are dramatically different to that obtained with the Wilson's equations. For instance, the location of the interferences is shifted. The first interference dip is at a frequency of 150 Hz using the Wilson's equations and at a frequency of 180 Hz using the Zwikker and Kosten's equations. As discussed in Wilson *et al.*, the Zwikker and Kosten's equations are not adapted for grounds with a low flow resistivity and should not be used in these cases.

Finally, the results obtained for a ground with an air flow resistivity $\sigma_0 = 200$ kPa s m^{-2} are examined. The time series of the pressure are shown in Fig. 10(a). The waveforms obtained by solving the Wilson's equations in the ground and obtained by using an impedance condition with the Wilson's model are almost superimposed. Moreover, some small discrepancies can be observed on the waveform obtained with the Zwikker and Kosten's equations, especially around $t = 0.436$ s. Concerning the ESD of the signal plotted as a function of the frequency in Fig. 10(b), it is observed that the ESD is the same when solving the Wilson's equations and using an equivalent impedance boundary condition. Indeed, the ground is hard enough so that the local reaction assumption is valid. The ESD obtained for the Zwikker and Kosten's equations is also not too far from that obtained with the Wilson's equations. It is retrieved that the Zwikker and Kosten's equations are valid for propagation over a grassy soil.

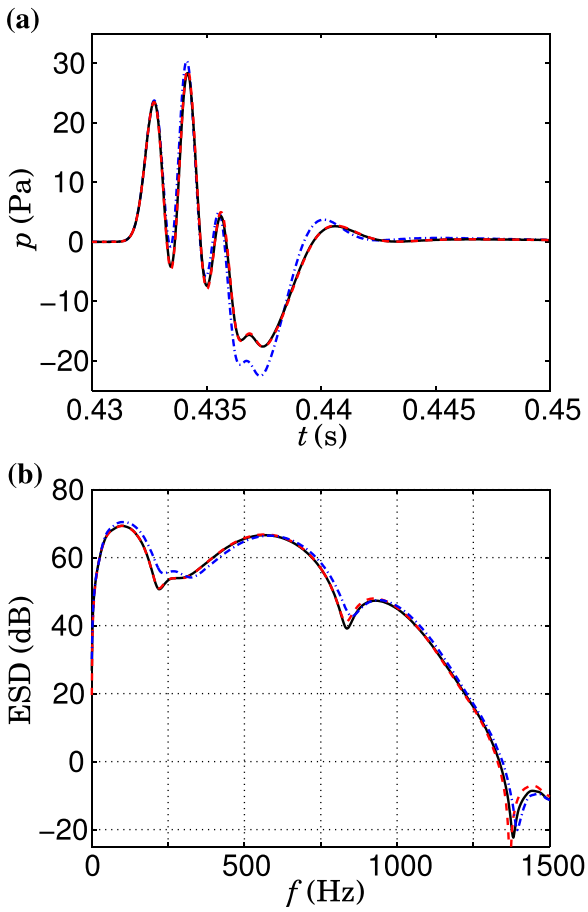

FIG. 10. (Color online) (a) Time series of the pressure and (b) corresponding energy spectral densities obtained at a receiver located at $x = 150$ m, $y = 0$ m, and $z = 2$ m for the three ground modelling: propagation in the ground using the (solid line) Wilson's and (dashed-dotted line) Zwikker and Kosten's equations, or (dashed line) impedance boundary condition using the Wilson's model. The air flow resistivity of the ground is set to $\sigma_0 = 200$ kPa s m^{-2}. The reference for the dB calculation is 4×10^{-10} Pa^2 s^2.

IV. CONCLUSION

Time-domain equations in porous media usually involve convolutions between relaxation functions and acoustic variables, which are not straightforward to compute. A method, referred to as the ADE method and originated from the electromagnetism and geophysics communities, was proposed to efficiently evaluate these convolutions. For this purpose, the relaxation functions are approximated by rational functions in the frequency domain. The convolution is replaced by a sum of new variables, called the auxiliary functions, whose time variations are governed by first-order partial differential equations. The accuracy of the ADE method was first investigated and compared to recursive convolution methods. It was shown that recursive methods are low order methods, while the ADE method does not modify the order of the time-integration scheme. Therefore, the ADE method is well-suited when employing high-order numerical schemes. The influence of the number of poles for the approximation of the relaxation function was then examined, showing that a few number of poles is typically sufficient to have accurate results. At last, the ADE method was applied to outdoor sound propagation using the equations of the Wilson's relaxation model to compute the propagation into the ground. A one-dimensional test-case was first considered to demonstrate the feasibility and the efficiency of the method. In particular, the computed characteristic impedance and attenuation in the ground were successfully compared to the analytical values. An application of the method to a 3D problem was then performed for two different types of ground and results were compared to those obtained using an equivalent impedance boundary condition or solving the Zwikker and Kosten's equations in the ground. For a very soft ground, the results substantially differ, in particular, close to the ground for the surface wave component. For a harder ground, the results obtained using the impedance boundary condition and the Wilson's relaxation equations in the ground are in close agreement while those obtained employing the Zwikker and Kosten's equations in the ground still slightly differ.

ACKNOWLEDGMENTS

This work was granted access to the HPC resources of IDRIS under the allocation 2014-022203 made by GENCI (Grand Equipement National de Calcul Intensif). It was performed within the framework of the Labex CeLyA of Université de Lyon, operated by the French National Research Agency (ANR-10-LABX-0060/ANR-11-IDEX-0007).

APPENDIX A: ANALYTICAL SOLUTION FOR THE INITIAL VALUE PROBLEM IN SEC. II

An analytical solution for the initial value problem proposed in Sec. II D 1 is here given. The equation is

$$\frac{\partial p}{\partial t} + c\frac{\partial p}{\partial x} + \hat{b}_\infty p - \hat{b}_\infty \lambda \phi = 0, \tag{A1}$$

with the initial value $p(x,\ t=0) = Q(x)$ and with $\phi(x,t) = \int_0^t e^{-\lambda(t-t')} p(x,t')\mathrm{d}t'$. Multiplying all terms by $e^{\lambda t}$, the preceding equation can be rewritten as

$$e^{\lambda t}\frac{\partial p}{\partial t} + ce^{\lambda t}\frac{\partial p}{\partial x} + \hat{b}_\infty e^{\lambda t} p - \hat{b}_\infty \lambda \int_0^t e^{\lambda t'} p(t')\mathrm{d}t' = 0. \tag{A2}$$

By derivating the equation and removing the factor $e^{\lambda t}$, one obtains

$$\frac{\partial^2 p}{\partial t^2} + \left(\lambda + \hat{b}_\infty\right)\frac{\partial p}{\partial t} + c\frac{\partial^2 p}{\partial x \partial t} + c\lambda\frac{\partial p}{\partial x} = 0. \tag{A3}$$

Introducing the spatial Fourier transform

$$\tilde{p}(k,t) = \int_{-\infty}^{\infty} p(x,t)e^{-ikx}\mathrm{d}x, \tag{A4}$$

Eq. (A3) becomes

$$\frac{\partial^2 \tilde{p}}{\partial t^2} + \left(\lambda + \hat{b}_\infty + ikc\right)\frac{\partial \tilde{p}}{\partial t} + ikc\lambda\tilde{p} = 0. \tag{A5}$$

Using the initial conditions

$$\tilde{p}(k,t=0) = \tilde{Q}(k), \quad \frac{\partial \tilde{p}}{\partial t}(k,t=0) = -\left(ikc + \hat{b}_\infty\right)\tilde{Q}(k), \tag{A6}$$

where $\tilde{Q}(k)$ is the Fourier transform of $Q(x)$, the solution is

$$p(x,t) = \frac{1}{2\pi}\int_{-\infty}^{\infty} \tilde{Q}\left[A_+ \exp(\omega_+ t) + A_- \exp(\omega_- t)\right]e^{ikx}\mathrm{d}k, \tag{A7}$$

with

$$\omega_\pm = \frac{1}{2}\left(-\lambda - \hat{b}_\infty - ikc \pm \sqrt{\left(\lambda + \hat{b}_\infty + ikc\right)^2 - 4ikc\lambda}\right), \tag{A8}$$

$$A_\pm = \frac{\omega_\mp + ikc + \hat{b}_\infty}{\omega_\pm - \omega_\mp}. \tag{A9}$$

Using Eq. (13), the analytical solution for ϕ is straightforwardly deduced, yielding

$$\phi(x,t) = \frac{1}{2\pi}\int_{-\infty}^{\infty} \tilde{Q}\left[\frac{A_+}{\omega_+ + \lambda}\exp(\omega_+ t) + \frac{A_-}{\omega_- + \lambda}\exp(\omega_- t)\right]e^{ikx}\mathrm{d}k. \tag{A10}$$

APPENDIX B: ANALYTICAL SOLUTION FOR THE ZWIKKER AND KOSTEN ADVECTION EQUATION

An analytical solution is proposed for the Zwikker and Kosten's advection equation:

$$\frac{\partial p}{\partial t} + \frac{c}{q}\frac{\partial p}{\partial x} + \frac{c}{q}\left[s * \frac{\partial p}{\partial x}\right] + \omega_0 p = 0, \tag{B1}$$

with $p(x, t=0) = Q(x)$. Introducing the Fourier-Laplace transform

$$\bar{p}(k,\omega) = \int_0^{+\infty}\int_{-\infty}^{+\infty} p(x,t)e^{i\omega t - ikx}\mathrm{d}x\,\mathrm{d}t, \tag{B2}$$

Eq. (B1) becomes

$$\bar{p}(k,\omega) = \frac{\tilde{Q}(k)}{D(\omega,k)}, \tag{B3}$$

where $\tilde{Q}(k)$ is the Fourier transform of $Q(x)$ and $D(\omega, k)$ is the dispersion equation

$$D(\omega,k) = \omega_0 - i\omega + \frac{ikc}{q}\sqrt{1 + \frac{\omega_0}{-i\omega}}. \tag{B4}$$

The branch cut of the square root function is chosen as the negative real axis, so that the branch cut corresponds in the ω-plane to the line segment $\mathrm{Re}[\omega] = 0$ and $\mathrm{Im}[\omega] \in [-\omega_0,\ 0]$. The dispersion equation has two zeros both located in the lower half ω-plane. The first one is located at $-i\omega_0$ and is not of interest here. The second one, denoted by ω_+ is purely imaginary if $|k|c/q < \omega_0/2$ and is located on the branch-cut at

$$\omega_+ = -\frac{i\omega_0}{2} + i\sqrt{\frac{\omega_0^2}{4} - \frac{k^2c^2}{q^2}}. \tag{B5}$$

If $|k|c/q > \omega_0/2$, it is located on the lower half-plane at

$$\omega_+ = -\frac{i\omega_0}{2} + \frac{kc}{q}\sqrt{1 - \frac{\omega_0^2 q^2}{4c^2k^2}}. \tag{B6}$$

The pressure in the time-domain can then be obtained by the transform

$$p(x,t) = \frac{1}{4\pi^2}\int_{-\infty}^{+\infty}\int_{-\infty}^{+\infty} \bar{p}(k,\omega)e^{-i\omega t + ikx}\mathrm{d}\omega\,\mathrm{d}k. \tag{B7}$$

The ω-integral can first be evaluated using the contour represented in Fig. 11. The acoustic field is a sum of two contributions $p = p_{\mathrm{bc}} + p_+$. The term p_{bc} is the contribution of the branch cut

$$p_{\mathrm{bc}}(x,t) = \frac{1}{4\pi^2}\int_{-\infty}^{+\infty} \tilde{p}_{\mathrm{bc}}(k,t)e^{ikx}\mathrm{d}k, \tag{B8}$$

with

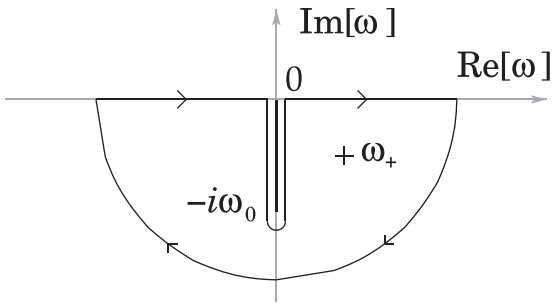

FIG. 11. Inversion contour and pole in the complex ω-plane.

$$\tilde{p}_{\rm bc}(k,t) = \int_{\epsilon}^{-i\omega_0+\epsilon} \frac{\tilde{Q}(k)}{D(\omega,k)}\,{\rm d}\omega + \int_{-i\omega_0-\epsilon}^{-\epsilon} \frac{\tilde{Q}(k)}{D(\omega,k)}\,{\rm d}\omega, \tag{B9}$$

where $\epsilon > 0$ is a small parameter. As ϵ tends to 0, the last equation can be rewritten as

$$\tilde{p}_{\rm bc}(k,t) = -\tilde{Q}(k)\int_0^1 e^{-\omega_0 vt}\frac{\sqrt{v}}{\sqrt{1-v}}\frac{2ikcq\omega_0}{q^2\omega^2(1-v)v - k^2c^2}\,{\rm d}v. \tag{B10}$$

It represents a stationary wave which decays exponentially with time. The second contribution to the acoustic field p_+ is a propagating wave, which is obtained from the zero of the dispersion equation, yielding

$$p_+(x,t) = \frac{1}{2\pi}\int_{-\infty}^{+\infty}\frac{-2i\omega_+\tilde{Q}(k)}{\omega_0 - 2i\omega_+}e^{-i\omega_+ t}e^{ikx}{\rm H}\left[\frac{|k|c}{q} - \frac{\omega_0}{2}\right]{\rm d}k. \tag{B11}$$

APPENDIX C: PATCHING TECHNIQUES

The patching techniques used to transmit information through the two subdomains, corresponding to the air and to the porous medium, are described in the case of Wilson's equations. For this purpose, the characteristic variables are determined from the equations in Eqs. (48)–(51) after having introduced the ADE equations. These equations are rewritten in the form

$$\frac{\partial \mathbf{U}}{\partial t} + \mathbf{A}\frac{\partial \mathbf{U}}{\partial x} + \mathbf{B}\frac{\partial \mathbf{U}}{\partial y} + \mathbf{C}\frac{\partial \mathbf{U}}{\partial z} + \mathbf{D}\mathbf{U} = 0, \tag{C1}$$

where $\mathbf{U}$ is the vector of unknown variables:

$$\mathbf{U} = [\mathbf{v} \quad p \quad \boldsymbol{\phi}_{\boldsymbol{k}}^{\boldsymbol{v}} \quad \phi_k^e]^T. \tag{C2}$$

Without loss of generality, one considers two media whose interface is located along the x axis at $x = 0$. The characteristic variables are obtained by diagonalizing the matrix $\mathbf{A} = \mathbf{P}\Lambda\mathbf{P}^{-1}$, where Λ is a diagonal matrix whose diagonal contains all the eigenvalues of $\mathbf{A}$ and $\mathbf{P}$ is a matrix whose columns are the corresponding eigenvectors. For a 3D geometry, the eigenvalues of the matrix $\mathbf{A}$ are c/q, $-c/q$, and 0, which is repeated $2 + 3N^v + N^e$ times. Equation (C1) can thus be rewritten as

$$\frac{\partial \tilde{\mathbf{U}}}{\partial t} + \Lambda\frac{\partial \tilde{\mathbf{U}}}{\partial x} + \mathbf{S} = 0, \tag{C3}$$

where $\tilde{\mathbf{U}} = \mathbf{P}^{-1}\mathbf{U}$ is the vector of characteristic variables and $\mathbf{S}$ is a matrix which depend on $\tilde{\mathbf{U}}$, $\partial/\partial y$, and $\partial/\partial z$ but does not depend on $\partial/\partial x$. Therefore, the characteristic variables $u^{\rightarrow}$ and $u^{\leftarrow}$, associated to the eigenvalues c/q and $-c/q$ represent outgoing and incoming waves traveling along the x-direction, respectively. Simple algebraic manipulations show that they are given by

$$u^{\leftarrow} = p - \frac{\rho_0 cq}{\Omega}v_x, \tag{C4}$$

$$u^{\rightarrow} = p + \frac{\rho_0 cq}{\Omega}v_x. \tag{C5}$$

The other characteristic variables associated to the eigenvalue 0 do not propagate in the x-direction. Note that the characteristic variables for the Zwikker and Kosten's equations have the same expressions.

Therefore, at the interface of the two media with different properties, the outgoing characteristic variable $u_1^{\rightarrow}$ in medium 1 located at $x < 0$ and the incoming characteristic variable $u_2^{\leftarrow}$ in medium 2 located at $x > 0$ are computed at each step of the Runge-Kutta algorithm. Imposing the continuity of the pressure and normal velocity at the interface, the acoustic variables are thus updated using the characteristic variables. For instance, if the medium 1 is a porous medium with a tortuosity q and a porosity Ω and if the medium 2 corresponds to air, the pressure and normal velocity at the interface are computed from

$$p = \frac{\Omega u_1^{\rightarrow} + q u_2^{\leftarrow}}{\Omega + q}, \tag{C6}$$

$$v_x = \frac{\Omega}{\rho_0 c_0}\frac{u_1^{\rightarrow} - u_2^{\leftarrow}}{\Omega + q}, \tag{C7}$$

with $u_1^{\rightarrow} = p + \rho_0 c v_x q/\Omega$ and $u_2^{\leftarrow} = p - \rho_0 c v_x$. The other acoustic variables are left unchanged.

Attenborough, K., Bashir, I., and Taherzadeh, S. (**2011**). "Outdoor ground impedance models," J. Acoust. Soc. Am. **129**, 2806–2819.

Berland, J., Bogey, C., and Bailly, C. (**2006**). "Low-dissipation and low-dispersion fourth-order Runge-Kutta algorithm," Comp. Fluids **35**, 1459–1463.

Bin, J., Hussaini, M. Y., and Lee, S. (**2009**). "Broadband impedance boundary conditions for the simulation of sound propagation in the time domain," J. Acoust. Soc. Am. **125**(2), 664–675.

Blanc, E., Chiavassa, G., and Lombard, B. (**2013**). "A time-domain numerical modeling of two-dimensional wave propagation in porous media with frequency-dependent dynamic permeability," J. Acoust. Soc. Am. **134**(6), 4610–4623.

Bogey, C., and Bailly, C. (**2004**). "A family of low dispersive and low dissipative explicit schemes for flow and noise computations," J. Comp. Phys. **194**, 194–214.

Botteldooren, D. (**1997**). "Vorticity and entropy boundary conditions for acoustical finite-difference time-domain simulations," J. Acoust. Soc. Am. **102**(1), 170–178.

Boyd, J. P. (**2001**). *Chebyshev and Fourier Spectral Methods*, 2nd ed. (Denver Publications Inc., Denver, CO), Chap. 2, pp. 19–60.

Carcione, J. M. (**2001**). *Wave Fields in Real Media: Wave Propagation in Anisotropic, Anelastic and Porous Media* (Pergamon, New York), 337 pp.

Cardoso, L., Teboul, F., Sedel, L., Oddou, C., and Meunier, A. (**2003**). "In vitro acoustic waves propagation in human and bovine cancellous bone," J. Bone Miner. Res. **18**(10), 1803–1812.
Cotté, B., Blanc-Benon, P., Bogey, C., and Poisson, F. (**2009**). "Time-domain impedance boundary conditions for simulations of outdoor sound propagation," AIAA J. **47**, 2391–2403.
Day, S. M., and Minster, J. B. (**1984**). "Numerical simulation of attenuated wavefields using a Padé approximant method," Geophys. J. R. Astro. Soc. **78**, 105–118.
Dragna, D., Blanc-Benon, P., and Poisson, F. (**2013**). "Time-domain solver in curvilinear coordinates for outdoor sound propagation over complex terrain," J. Acoust. Soc. Am. **133**, 3751–3763.
Dragna, D., Cotté, B., Blanc-Benon, P., and Poisson, F. (**2011**). "Time-domain simulations of outdoor sound propagation with suitable impedance boundary conditions," AIAA J. **49**, 1420–1428.
Fellah, M., Fellah, Z. E. A., Mitri, F. G., Ogam, E., and Depollier, C. (**2013**). "Transient ultrasound propagation in porous media using Biot theory and fractional calculus: Application to human cancellous bone," J. Acoust. Soc. Am. **133**(4), 1867–1881.
Fellah, Z. E. A., Berger, S., Lauriks, W., Depollier, C., Aristegui, C., and Chapelon, J.-Y. (**2003**). "Measuring the porosity and the tortuosity of porous materials via reflected waves at oblique incidence," J. Acoust. Soc. Am. **113**(5), 2424–2433.
Fellah, Z. E. A., Chapelon, J.-Y., Berger, S., Lauriks, W., and Depollier, C. (**2004**). "Ultrasonic wave propagation in human cancellous bone: Application of Biot theory," J. Acoust. Soc. Am. **116**(1), 61–73.
Groby, J. P., and Tsogka, C. (**2006**). "A time domain method for modeling viscoacoustic wave propagation," J. Comp. Acoust. **14**(2), 201–236.
Gustavsen, B., and Semlyen, A. (**1999**). "Rational approximation of frequency domain responses by vector fitting," IEEE Trans. Power Delivery **14**(3), 1052–1061.
Haïat, G., Padilla, F., Peyrin, F., and Laugier, P. (**2008**). "Fast wave ultrasonic propagation in trabecular bone: Numerical study of the influence of porosity and structural anisotropy," J. Acoust. Soc. Am. **123**(3), 1694–1705.
Hornikx, M. (**2009**). "Numerical modelling of sound propagation to closed urban courtyards," Doctoral thesis, Chalmers University of Technology, Gothenburg, Sweden, pp. 133–137.
Hornikx, M., Waxler, R., and Forssén, J. (**2010**). "The extended Fourier pseudospectral time-domain method for atmospheric sound propagation," J. Acoust. Soc. Am. **128**, 1632–1646.
Joseph, R. M., Hagness, S. C., and Taflove, A. (**1991**). "Direct time integration of Maxwell's equations in linear dispersive media with absorption for scattering and propagation of femtosecond electromagnetic pulses," Opt. Lett. **16**, 1412–1414.
Kelley, D. F., and Luebbers, R. J. (**1996**). "Piecewise linear recursive convolution for dispersive media using FDTD," IEEE Trans. Antennas Propag. **44**(6), 792–797.
Li, X. Y., Li, X. D., and Tam, C. K. W. (**2012**). "Improved multipole broadband time-domain impedance," AIAA J. **50**(4), 980–984.
Luebbers, R. J., and Hunsberger, F. (**1992**). "FDTD for Nth-order dispersive media," IEEE Trans. Antennas Propag. **40**, 1297–1301.
Ostashev, V. E., Collier, S. L., Wilson, D. K., Aldridge, D. F., Symons, N. P., and Marlin, D. H. (**2007**). "Padé approximation in time-domain boundary conditions of porous surfaces," J. Acoust. Soc. Am. **122**(1), 107–112.
Ostashev, V. E., Wilson, D. K., Liu, L., Aldridge, D. F., Symons, N. P., and Marlin, D. (**2005**). "Equations for finite-difference, time-domain simulation of sound propagation in moving inhomogeneous media and numerical implementation," J. Acoust. Soc. Am. **117**, 503–517.
Özyörük, Y., and Long, L. N. (**1996**). "A time-domain implementation of surface acoustic impedance condition with and without flow," J. Comp. Acoust. **5**(3), 277–296.
Reymen, Y., Baelmans, M., and Desmet, W. (**2008**). "Efficient implementation of Tam and Auriault's time-domain impedance boundary condition," AIAA J. **46**(9), 2368–2376.
Salomons, E. (**2001**). *Computational Atmospheric Acoustics* (Kluwer Academic Publishers, Dordrecht), 118 p.
Salomons, E. M., Blumrich, R., and Heimann, D. (**2002**). "Eulerian time-domain model for sound propagation over a finite-impedance ground surface. Comparison with frequency-domain models," Acta Acust. Acust. **88**, 483–492.
Siushansian, R., and LoVetri, J. (**1997**). "Efficient evaluation of convolution integrals arising in FDTD formulations of electromagnetic dispersive media," J. Electromag. Waves Appl. **11**, 101–117.
Sullivan, D. M. (**1992**). "Frequency-dependent FDTD methods using Z transforms," IEEE Trans. Antennas Propag. **40**(10), 1223–1230.
Sullivan, D. M. (**1996**). "Z-transform theory and the FDTD method," IEEE Trans. Antennas Propag. **44**(1), 28–34.
Umnova, O., and Turo, D. (**2009**). "Time domain formulation of the equivalent fluid model for rigid porous media," J. Acoust. Soc. Am. **125**, 1860–1863.
Van Renterghem, T., and Botteldooren, D. (**2003**). "Numerical simulation of the effect of trees on downwind noise barrier performance," Acta Acust. Acust. **89**, 764–778.
Wilson, D. K., Ostashev, V. E., Collier, S. L., Symons, N. P., Aldridge, D. F., and Marlin, D. H. (**2007**). "Time-domain calculations of sound interactions with outdoor ground surfaces," Appl. Acoust. **68**, 173–200.